Suitable Single-Phase to Three-Phase AC–DC–AC Power Conversion System

Euzeli Cipriano dos Santos Jr., *Senior Member, IEEE*, Nady Rocha, *Member, IEEE*, and Cursino Brandão Jacobina, *Fellow, IEEE*

***Abstract*—This paper presents a single-phase to three-phase power conversion system with parallel rectifier and series inverter to cope with single-phase to three-phase asymmetry. Such converter guarantees both reduction in the input current processed by rectifier circuit and reduction of the output voltage processed by the inverter circuit. It is worth mentioning that, in spite of proposing a topology with features not yet observed on the technical literature, this paper presents a comprehensive model of the proposed converter, modulation strategy, and a general comparison with the conventional configuration. Simulated and experimental results are also presented.**

***Index Terms*—Power conversion, power electronics converters, pulse width modulation converters.**

I. Introduction

In the past, single-phase to three-phase conversion systems were made possible by the connection of passive elements (capacitors and reactors) with autotransformer converters [1]–[3]. Such kind of system presents well-known disadvantages and limitations [3]. In those days, power electronics with silicon power diodes and thyristors was just emerging. As described in [4], the so-called power electronics, with gas tube and glass-bulb electronics, was known as industrial electronics, and the power electronics with silicon-controlled rectifiers began emerging in the market from the early 1960s.

Since the beginning of the solid state power electronics, the semiconductor devices were the major technology used to drive the power processors [5]. Looking at the semiconductor devices used in the former controlled rectifiers [6] and comparing them with the new technologies [7], it makes possible to figure out the astonishing development. Beyond the improvement related to power switches, it was also identified a great activity in terms of the circuit topology innovations in the field of three-phase to three-phase, single-phase to single-phase, and three-phase to single-phase conversion systems [8].

Manuscript received November 25, 2013; revised February 4, 2014; accepted February 14, 2014. Date of publication February 28, 2014; date of current version October 7, 2014. Recommended for publication by Associate Editor J. R. Espinoza.

E. C. dos Santos, Jr. is with the Department of Electrical and Computer Engineering, Indiana University—Purdue University Indianapolis, Indianapolis, IN 46202 USA (e-mail: euzeli.santos@gmail.com).

N. Rocha is with the Department of Electrical Engineering, Federal University of Paraíba, 58051-900 João Pessoa, Brazil (e-mail: nadyrocha@gmail.com).

C. B. Jacobina is with the Department of Electrical Engineering, Federal University of Campina Grande, Campina Grande 58109-970 Paraiba, Brazil (e-mail: jacobina@dee.ufcg.edu.br).

Color versions of one or more of the figures in this paper are available online at http://ieeexplore.ieee.org.

Digital Object Identifier 10.1109/TPEL.2014.2308297

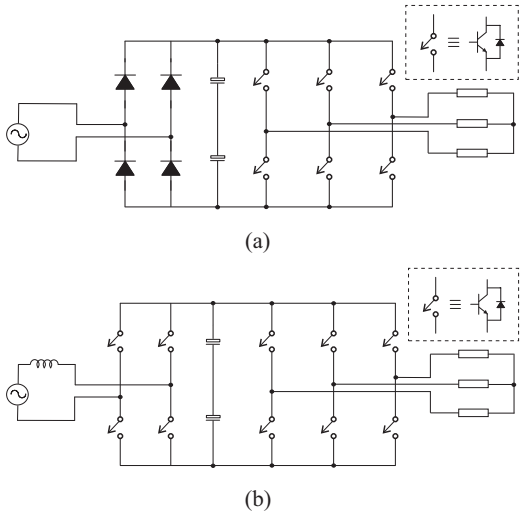

Fig. 1. Conventional single-phase to three-phase configurations: (a) diode bridge at the input-converter side, and (b) controlled rectifier at the input-converter side.

In the power distribution systems, the single-phase grid [9] has been considered as an alternative for rural or remote areas [10], due to its lower cost feature, especially when compared with the three-phase solution. In huge countries like Brazil [11], the single-phase grid is quite common due to the large area to be covered. On the other hand, loads connected in a three-phase arrangement presents some advantages when compared to single-phase loads. This is especially true in three-phase motor systems with variable-speed drives due to their constant torque characteristic [12]–[14]. In this scenario, there is a need for single-phase to three-phase power conversion systems. The direct solutions for the single-phase to three-phase power converters are presented in Fig. 1. Fig. 1(b) shows a solution for single-phase to three-phase power conversion, in which all variables (e.g., input power factor and dc-link voltage) at input–output converter sides can be controlled, as observed in Fig. 2(b). On the other hand, the configuration presented in Fig. 1(a) represents a cheaper solution but without any control of the input current and dc-link voltage, as observed in Fig. 2(a).

In general terms, a single-phase to three-phase power conversion presents an inherent asymmetry, i.e., constant power at the output-converter side (three-phase load) and pulsating power at the input-converter side (single-phase grid), as highlighted in Fig. 3(a). The direct consequence of this asymmetry is the low-frequency voltage oscillation observed in the dc-link capacitors, as well as the power switches of the rectifier and inverter operate with different voltage and current ratings. Normally, the

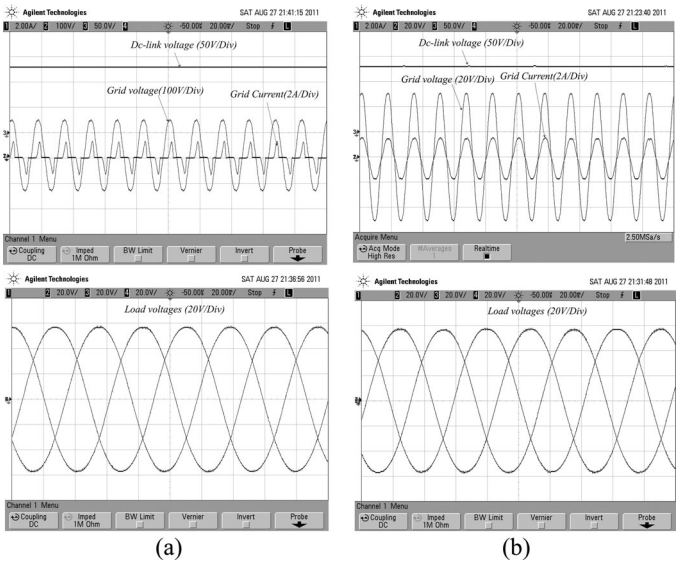

Fig. 2. Experimental results of the conventional single-phase to three-phase power conversion. (a) Configuration presented in Fig. 1(a). (b) Configuration presented in Fig. 1(b).

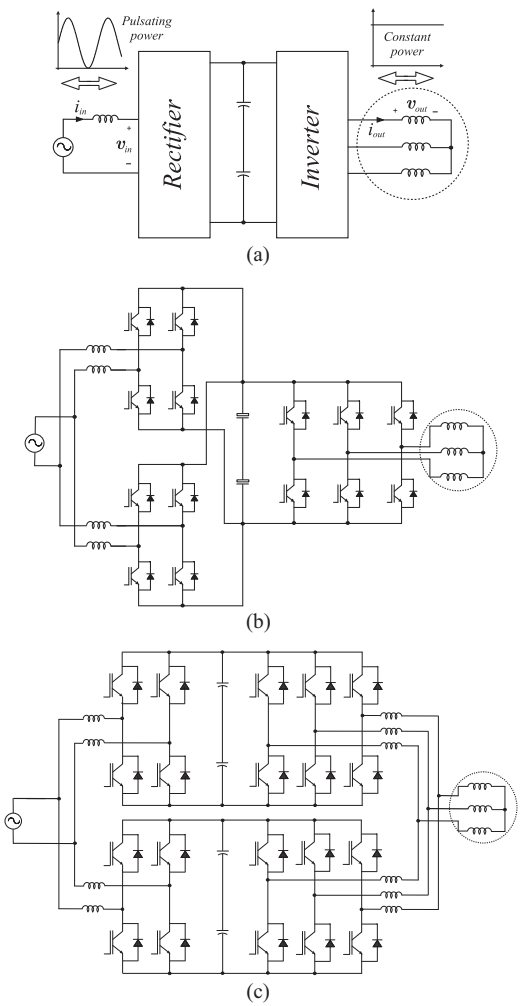

Fig. 3. Single-phase to three-phase power conversion. (a) Type of power processed by rectifier and inverter circuits. (b) Solution employed in [15]. (c) Solution employed in [16].

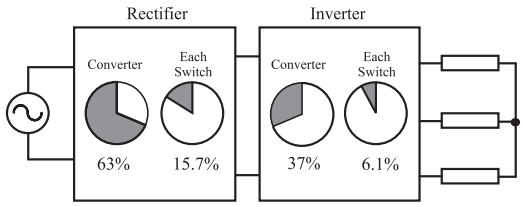

Fig. 4. Converter power losses distribution in both rectifier and inverter units: 63% in the rectifier circuit and 37% in the inverter one. Power losses in each switch of the rectifier (15.7%) and inverter (6.1%).

three-phase motor-rated voltage is higher than that furnished by the single-phase grid (considering the Brazilian voltages available, it is possible to identify: $v_{\rm in} = 110$ V, $v_{\rm out} = 220$ V, or $v_{\rm in} = 220$ V, $v_{\rm out} = 220$ V - depending of the region), which means that the rectifier circuit must boost the grid voltage to guarantee the motor-rated voltage. Furthermore, the current relation between input- and output-converter sides also implies in converter asymmetry, i.e., ($i_{\rm in} > i_{\rm out}$).

Another important characteristic observed in the single-phase to three-phase power converters that also has been considered in this paper is the irregular distribution of power losses among the switches of the converter, as observed in Fig. 4. It means that, for a 600 V 50A class of insulated gate bipolar transistor (IGBT), 63% of the total losses measured in the single-phase to three-phase converter is concentrated in the rectifier circuit, while the rest 37% is observed in the inverter circuit. With those numbers, it is possible to measure the stress by switch, which means that each rectifier switch is responsible for 15.7% of the total converter losses, while each inverter switch is responsible for only 6.1%. The loss per switch gives an important parameter regarding the possibilities of failures in the power converters.

Many configurations have been considered to deal with this asymmetry, as in [15] in which a parallel rectifier circuit is considered to reduce the current processed by rectifier switches [see Fig. 3(b)], as well as to improve the harmonic distortion, reliability, and efficiency at the input-converter side. With the same philosophy, Jacobina *et al.* [16] proposes two single-phase to three-phase ac–dc–ac converters paralleled [see Fig. 3(c)], meaning improvements at input–output converter sides. To handle with the low-frequency voltage fluctuation observed in the dc-link voltage, Ohnuma and Itoh in [17] and [18] present a configuration with a specific control method for a single-phase to three-phase power converter with power decoupling function. None of the configurations observed in the technical literature, solve the whole asymmetry inherent of the single-phase to three-phase power conversion, i.e., higher input current ($i_{\rm in}$) and a demand for higher output voltage ($v_{\rm out}$). Indeed, the configurations observed in Fig. 3(b) and 3(c) reduce the current processed by the rectifier current, but the voltage at the output converter remains the same as in Fig. 1(b).

This paper presents a single-phase to three-phase power conversion system with parallel rectifier and series inverter to cope with single-phase to three-phase asymmetry, as observed in Fig. 5. Such converter guarantees both reduction in the input current processed by rectifier circuit (due to the parallel connection) and reduction of the output voltage processed by each

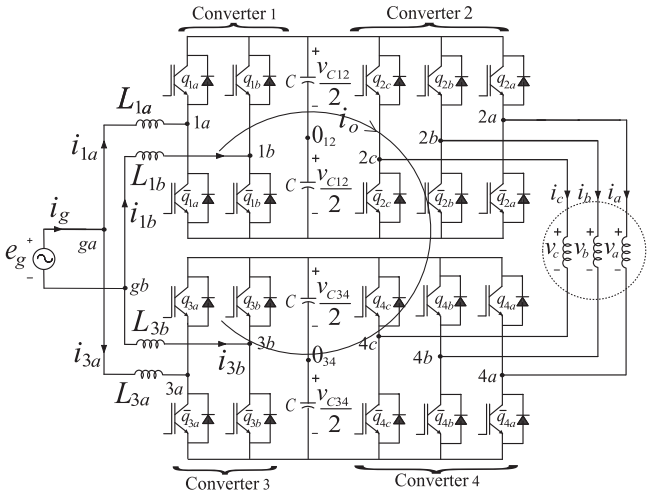

Fig. 5. Proposed single-phase to three-phase conversion system.

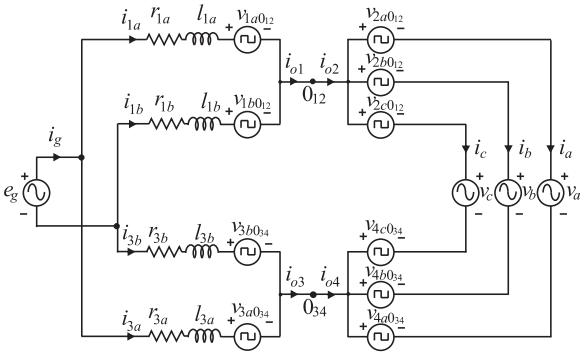

Fig. 6. Simplified model of the proposed single-phase to three-phase conversion system.

inverter (due to the series connection). It is worth mentioning that, in spite of proposing a topology with features not yet observed in the technical literature, this paper presents a comprehensive model of the proposed converter, modulation strategy, and a general comparison with the conventional configuration. Experimental results are used for the validation purpose.

II. System Model

This section will present the model of the proposed configuration. Such a configuration is constituted by a single-phase grid (e_g), one open-end three-phase motor, inductor filters (L_{1a}, L_{1b}, L_{3b}, and L_{3a}), converters 1, 2, 3, and 4, and two dc-link capacitor banks (C_{12} and C_{34}). If the legs are substituted by pulsed voltage sources, the proposed converter can be modeled as in Fig. 6.

A. Grid-Side Converter Model

From the system in Fig. 6, the following equations can be derived to converters 1 and 3 at the grid side:

$$e_g = r_{1a} i_{1a} + l_{1a} \frac{di_{1a}}{dt} - r_{1b} i_{1b} - l_{1b} \frac{di_{1b}}{dt} + v_1 \tag{1}$$

$$e_g = r_{3a} i_{3a} + l_{3a} \frac{di_{3a}}{dt} - r_{3b} i_{3b} - l_{3b} \frac{di_{3b}}{dt} + v_3 \tag{2}$$

$$i_g = i_{1a} + i_{3a} \tag{3}$$

with

$$v_1 = v_{1a0_{12}} - v_{1b0_{12}} \tag{4}$$

$$v_3 = v_{3a0_{34}} - v_{3b0_{34}} \tag{5}$$

where i_{1a} and i_{1b} are the input currents of the converter 1, i_{3a} and i_{3b} are the input currents of the converter 3, the symbols r and l represent the resistance and inductance of inductors L_{1a}, L_{1b}, L_{3a}, and L_{3b}. The voltages $v_{1a0_{12}}$ and $v_{1b0_{12}}$ are the pole voltages of the converter 1, while $v_{3a0_{34}}$ and $v_{3b0_{34}}$ are the pole voltages of the converter 3 and i_g is the grid current.

B. Machine-Side Converter Model

From the system in Fig. 6, the following equations can be derived to converters 2 and 4 at the machine side:

$$v_{ab} = v_{2a0_{12}} - v_{2b0_{12}} + v_{4b0_{34}} - v_{4a0_{34}} \tag{6}$$

$$v_{bc} = v_{2b0_{12}} - v_{2c0_{12}} + v_{4c0_{34}} - v_{4b0_{34}} \tag{7}$$

$$v_{ca} = v_{2c0_{12}} - v_{2a0_{12}} + v_{4a0_{34}} - v_{4c0_{34}} \tag{8}$$

where $v_{2a0_{12}}$, $v_{2b0_{12}}$, and $v_{2c0_{12}}$ are the pole voltages of converter 2, $v_{4a0_{34}}$, $v_{4b0_{34}}$, and $v_{4c0_{34}}$ are the pole voltages of converter 4, and $v_{ab} = v_a - v_b$, $v_{bc} = v_b - v_c$, and $v_{ca} = v_c - v_a$ are line-to-line voltages of the machine.

For the voltage control of the motor, the following relations are obtained:

$$v_{2ab} = v_{2a0_{12}} - v_{2b0_{12}} = \frac{v_{ab}}{2} \tag{9}$$

$$v_{2bc} = v_{2b0_{12}} - v_{2b0_{12}} = \frac{v_{bc}}{2} \tag{10}$$

$$v_{2ca} = v_{2c0_{12}} - v_{2a0_{12}} = \frac{v_{ca}}{2} \tag{11}$$

$$v_{4ab} = v_{4a0_{34}} - v_{4b0_{34}} = -\frac{v_{ab}}{2} \tag{12}$$

$$v_{4bc} = v_{4b0_{34}} - v_{4c0_{34}} = -\frac{v_{bc}}{2} \tag{13}$$

$$v_{4ca} = v_{4c0_{34}} - v_{4a0_{34}} = -\frac{v_{ca}}{2}. \tag{14}$$

C. Circulating Current Model

Due to the parallel/series connection, the proposed system shown in Fig. 5 has a circulating current among the converts. The model of this circulating current can be defined as following:

$$0 = v_{za} + v_{1a0_{12}} - v_{3a0_{34}} + v_{2j0_{12}} - v_{4j0_{34}} + v_j \tag{15}$$

$$0 = v_{zb} + v_{1b0_{12}} - v_{3b0_{34}} + v_{2j0_{12}} - v_{4j0_{34}} + v_j \tag{16}$$

with $j = a, b, c$ and

$$v_{za} = r_{1a} i_{1a} + l_{1a} \frac{di_{1a}}{dt} - r_{3a} i_{3a} - l_{3a} \frac{di_{3a}}{dt} \tag{17}$$

$$v_{zb} = r_{1b} i_{1b} + l_{1b} \frac{di_{1b}}{dt} - r_{3b} i_{3b} - l_{3b} \frac{di_{3b}}{dt}. \tag{18}$$

The equations of the input circulating currents of the converters 1 and 3 (i_{o1} and i_{o3}) and output circulating currents of the converters 2 and 4 (i_{o2} and i_{o4}) are defined as

$$i_{o1} = i_{1a} + i_{1b} \tag{19}$$

$$i_{o2} = i_{2a} + i_{2b} + i_{2c} \tag{20}$$

$$i_{o3} = i_{3a} + i_{3b} \tag{21}$$

$$i_{o4} = i_{4a} + i_{4b} + i_{4c}. \tag{22}$$

However, the circulating currents i_{o1}, i_{o2}, i_{o3}, and i_{o4} can be represented by a single circulating current i_o, which means

$$i_o = i_{o1} = i_{o2} = -i_{o3} = -i_{o4}. \tag{23}$$

From (15) and (16), it is possible to write

$$v_o = v_{o1} - v_{o3} + (r_{1b} + r_{3b})i_o + (l_{1b} + l_{3b})\frac{di_o}{dt} + \frac{2}{3}\sum_{j=a}^{c} v_j \tag{24}$$

with

$$v_{o1} = (r_{1a} - r_{1b})i_{1a} + (l_{1a} - l_{1b})\frac{di_{1a}}{dt} \tag{25}$$

$$v_{o3} = (r_{3a} - r_{3b})i_{3a} + (l_{3a} - l_{3b})\frac{di_{3a}}{dt} \tag{26}$$

$$v_o = \sum_{i=a}^{b} v_{1i0_{12}} + \frac{2}{3}\sum_{j=a}^{c} v_{2j0_{12}} + \sum_{i=a}^{b} v_{3i0_{34}} - \frac{2}{3}\sum_{j=a}^{c} v_{4j0_{34}}. \tag{27}$$

D. Three-Phase Motor Model

A typical three-phase machine has been used in this study. Selecting a fixed coordinate reference frame, the mathematical model that describes the dynamic behavior of the three-phase induction motor is given by

$$\mathbf{v}_{sdq} = r_s \mathbf{i}_{sdq} + \frac{d}{dt}\phi_{sdq} \tag{28}$$

$$\mathbf{v}_{rdq} = r_r \mathbf{i}_{rdq} + \frac{d}{dt}\phi_{rdq} - j\omega_r \phi_{rdq} \tag{29}$$

$$\phi_{sdq} = l_s \mathbf{i}_{sdq} + l_{sr} \mathbf{i}_{rdq} \tag{30}$$

$$\phi_{rdq} = l_{sr} \mathbf{i}_{sdq} + l_r \mathbf{i}_{rdq} \tag{31}$$

$$v_{so} = r_s i_{so} + l_{ls}\frac{d}{dt} i_{so} \tag{32}$$

$$v_{ro} = r_r i_{ro} + l_{lr}\frac{d}{dt} i_{ro} \tag{33}$$

$$T_e = P l_{sr}(i_{sq} i_{rd} - i_{sd} i_{rq}) \tag{34}$$

where $\mathbf{v}_{sdq} = v_{sd} + jv_{sq}$, $\mathbf{i}_{sdq} = i_{sd} + ji_{sq}$, and $\phi_{sdq} = \phi_{sd} + j\phi_{sq}$ are the voltage, current, and flux dq vectors of the stator, respectively; v_{so} and i_{so} are the homopolar voltage and current of the stator, respectively (the equivalent rotor variables are obtained by replacing the subscript s by r); T_e is the electromagnetic torque; ω_r is the angular frequency of the rotor; r_s and r_r are the stator and rotor resistances; l_s, l_{ls}, l_r, and l_{lr} are the self and leakage inductance of the stator and rotor, respectively; l_{sr} is the mutual inductance and P is the number of pole pairs of the machine.

The dqo stator variables of the previous model can be determined from the abc variables by using the transformation given by

$$w_{sdqo} = A_s w_{abc} \tag{35}$$

with $w_{sdqo} = [w_{sd}\ w_{sq}\ w_{so}]^T$, $w_{abc} = [w_a\ w_b\ w_c]^T$ and

$$A_s = \sqrt{\frac{2}{3}}\begin{bmatrix} 1 & -\frac{1}{2} & -\frac{1}{2} \\ 0 & \frac{\sqrt{3}}{2} & -\frac{\sqrt{3}}{2} \\ \frac{\sqrt{2}}{2} & \frac{\sqrt{2}}{2} & \frac{\sqrt{2}}{2} \end{bmatrix}.$$

Vectors w_{sdqo} and w_{abc} can be voltage or current or flux vectors and $A_s^{-1} = A_s^T$.

III. Modulation Strategy

The converter pole voltages depend on the conduction states of the power switches. For example, $v_{1a0_{12}}$ is given by

$$v_{1a0_{12}} = (2q_{1a} - 1)\frac{v_{C12}}{2} \tag{36}$$

where v_{C12} is the dc-link voltage connected between the converters 1 and 2; and q_{1a} is the switching state of the top switch for the leg on converter 1 connected to the inductor L_{1a}.

The reference pole voltages $v^*_{1a0_{12}}$ to $v^*_{4c0_{34}}$ should be calculated from the reference voltages defined by controllers, i.e., v_1^*, v_3^*, v_o^*, two among v^*_{2ab}, v_{2bc},* and v^*_{2ca} and two among v^*_{4ab}, v^*_{4bc}, and v^*_{4ca}, which yields

$$v_1^* = v^*_{1a0_{12}} - v^*_{1b0_{12}} \tag{37}$$

$$v_3^* = v^*_{3a0_{34}} - v^*_{3b0_{34}} \tag{38}$$

$$v^*_{2ab} = v^*_{2a0_{12}} - v^*_{2b0_{12}} \tag{39}$$

$$v^*_{2bc} = v^*_{2b0_{12}} - v^*_{2c0_{12}} \tag{40}$$

$$v^*_{4ab} = v^*_{4a0_{34}} - v^*_{4b0_{34}} \tag{41}$$

$$v^*_{4bc} = v^*_{4b0_{34}} - v^*_{4c0_{34}} \tag{42}$$

$$v_o^* = -\sum_{i=a}^{b} v^*_{1i0_{12}} + \frac{2}{3}\sum_{k=a}^{c} v^*_{2k0_{12}} + \sum_{i=a}^{b} v^*_{3i0_{34}} - \frac{2}{3}\sum_{k=a}^{c} v^*_{4k0_{34}}. \tag{43}$$

Since the proposed converter has ten power switches, (37) to (43) are not sufficient to determine the reference pole voltages, then three auxiliary variables v_x^*, v_y^*, and v_z^* are introduced, that is,

$$v_x^* = \frac{1}{2}(v^*_{1a0_{12}} + v^*_{1b0_{12}}) \tag{44}$$

$$v_y^* = \frac{1}{3}(v^*_{3a0_{34}} + v^*_{3b0_{34}}) \tag{45}$$

$$v_z^* = \frac{1}{3}(v^*_{2a0_{12}} + v^*_{2b0_{12}} + v^*_{2c0_{12}}). \tag{46}$$

The reference pole voltages can now be obtained directly from (37) to (46), that is

$$v^*_{1a0_{12}} = \frac{1}{2}v_1^* + v_x^* \tag{47}$$

$$v^*_{1b0_{12}} = -\frac{1}{2}v_1^* + v_x^* \tag{48}$$

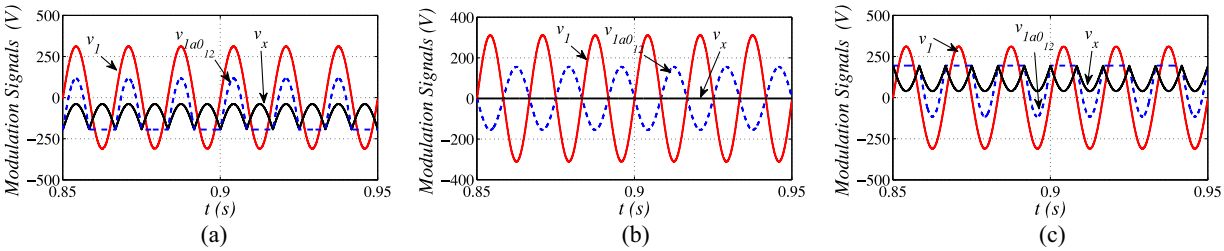

Fig. 7. Modulation signals at the grid side with: (a) $\mu_x = 0$, (b) $\mu_x = 0.5$, and (c) $\mu_x = 1$.

$$v^*_{2a0_{12}} = v^*_{2a} + v^*_z \tag{49}$$

$$v^*_{2b0_{12}} = v^*_{2b} + v^*_z \tag{50}$$

$$v^*_{2c0_{12}} = v^*_{2c} + v^*_z \tag{51}$$

$$v^*_{3a0_{34}} = \frac{1}{2}v^*_3 + v^*_y \tag{52}$$

$$v^*_{3b0_{34}} = -\frac{1}{2}v^*_3 + v^*_y \tag{53}$$

$$v^*_{4a0_{34}} = v^*_{4a} - \frac{1}{2}v^*_o + v^*_x - v^*_y + v^*_z \tag{54}$$

$$v^*_{4b0_{34}} = v^*_{4b} - \frac{1}{2}v^*_o + v^*_x - v^*_y + v^*_z \tag{55}$$

$$v^*_{4c0_{34}} = v^*_{4c} - \frac{1}{2}v^*_o + v^*_x - v^*_y + v^*_z \tag{56}$$

where

$$v^*_{2a} = -\frac{1}{3}v^*_{2ab} + \frac{1}{3}v^*_{2bc} \tag{57}$$

$$v^*_{2b} = -\frac{1}{3}v^*_{2ab} + \frac{1}{3}v^*_{2bc} \tag{58}$$

$$v^*_{2c} = -\frac{1}{3}v^*_{2ab} - \frac{2}{3}v^*_{2bc} \tag{59}$$

$$v^*_{4a} = -\frac{1}{3}v^*_{4ab} + \frac{1}{3}v^*_{4bc} \tag{60}$$

$$v^*_{4b} = -\frac{1}{3}v^*_{4ab} + \frac{1}{3}v^*_{4bc} \tag{61}$$

$$v^*_{4c} = -\frac{1}{3}v^*_{4ab} - \frac{2}{3}v^*_{4bc}. \tag{62}$$

To solve the problem of how to determine the reference pole voltages as a function of the reference voltages (v^*_1, v^*_3, v^*_o, v^*_{2ab}, v^*_{2bc}, v_{4ab},* and v^*_{4bc}), it is necessary to choose the auxiliary variables v^*_x, v_y,* and v^*_z appropriately. The auxiliary variables can be chosen freely in a range defined by the limits of the pole voltages $[v_{C12}/2,\ -v_{C12}/2]$ and $[v_{C34}/2,\ -v_{C34}/2]$.

In order to simplify the auxiliary variables calculation, the voltages v^*_x and v^*_y are first determined. From (47) and (48), the limit values for v^*_x is

$$v^*_{x\min} \le v^*_x \le v^*_{x\max} \tag{63}$$

$$v^*_{x\max} = v^*_{c12}/2 - \max\left\{\frac{v^*_1}{2}, -\frac{v^*_1}{2}\right\} \tag{64}$$

$$v^*_{x\min} = -v^*_{c12}/2 - \min\left\{\frac{v^*_1}{2}, -\frac{v^*_1}{2}\right\}. \tag{65}$$

Now, from (52) and (53), the limit values for v^*_y is

$$v^*_{y\min} \le v^*_y \le v^*_{y\max} \tag{66}$$

$$v^*_{y\max} = v^*_{c34}/2 - \max\left\{\frac{v^*_3}{2}, -\frac{v^*_3}{2}\right\} \tag{67}$$

$$v^*_{y\min} = -v^*_{c34}/2 - \min\left\{\frac{v^*_3}{2}, -\frac{v^*_3}{2}\right\}. \tag{68}$$

Given v^*_x and v^*_y, the limits of voltage v^*_z are determined from (49) and (51) and (54)–(56), i.e.,

$$v^*_{z\min} \le v^*_z \le v^*_{z\max} \tag{69}$$

$$v^*_{z\max} = v^*_c/2 - \max\{V_z\} \tag{70}$$

$$v^*_{z\min} = -v^*_c/2 - \min\{V_z\} \tag{71}$$

with $v^*_C = v^*_{C12} = v^*_{C34}$ and $V_z = \{v^*_{2a},\ v^*_{2b},\ v^*_{2c},\ v^*_{4a} - v^*_o/2 + v^*_x - v^*_y,\ v^*_{4b} - v^*_o/2 + v^*_x - v^*_y, v^*_{4c} - v^*_o/2 + v^*_x - v^*_y\}$.

Introducing the parameters μ_x, μ_y, and μ_z $(0 \le \mu \le 1)$, for instance, voltage v^*_x can be chosen equal to

$$v^*_x = \mu_x v^*_{x\max} + (1 - \mu_x)\, v^*_{x\min}. \tag{72}$$

The sequence for calculation of the reference pole voltages from v^*_1, v^*_3, v^*_o, v^*_{2ab}, v^*_{2bc}, v^*_{4ab}, and v^*_{4bc} is resumed in the following algorithm:

Step 1: 1) Determine $v^*_{x\max}$ and $v^*_{x\min}$ from (64) and (65); 2) choose μ_x; 3) determine v^*_x from (72).

Step 2: 1) Determine $v^*_{y\max}$ and $v^*_{y\min}$ from (67) and (68); 2) choose μ_y; 3) determine v^*_y from an equation similar to (72).

Step 3: 1) Determine $v^*_{z\max}$ and $v^*_{z\min}$ from (70) and (71); 2) choose μ_z; 3) determine v^*_z from an equation like (72).

Step 4: 1) Determine the reference pole voltages from (47) to (56).

Once the reference pole voltages have previously developed, the gating signals can be obtained by a comparison of the pole voltages with a high-frequency triangular carrier signal, as in [19]–[22]. In this paper, gating signals were obtained comparing pole voltages with a single or double-carrier-based pulse width modulation (PWM).

The parameters μ_x, μ_y, and μ_z change the place of the voltage pulses related to v_1, v_3, v_{ab}, v_{bc}, and v_{ca}. As an example, when $\mu_x = 0$ or $\mu_x = 1$ is selected, the pulses are placed at the beginning or at the end of the half period of the triangular carrier signal (T_s). On the other hand, when $\mu_x = 0.5$, the

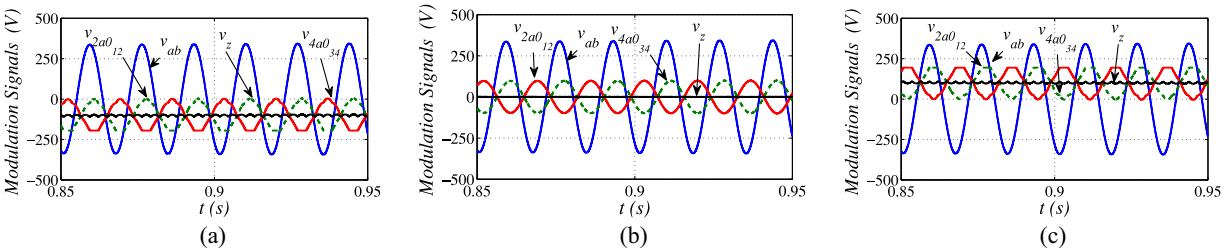

Fig. 8. Modulation signals at the machine side: (a) $\mu_z = 0$, (b) $\mu_z = 0.5$, and (c) $\mu_z = 1$.

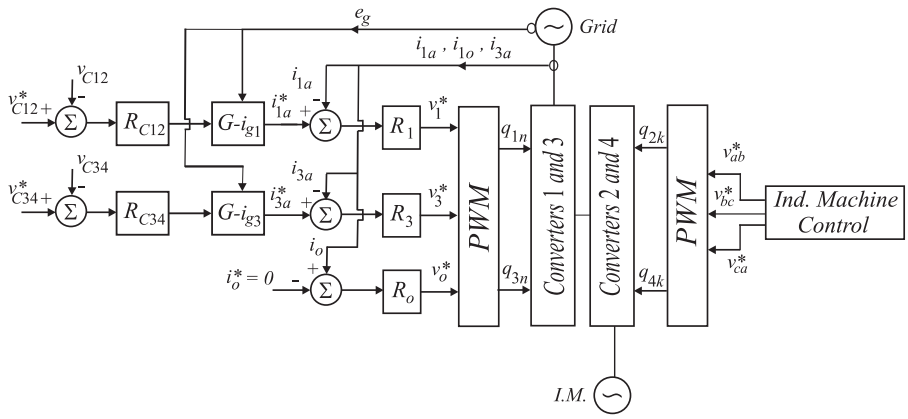

Fig. 9. Control block diagram.

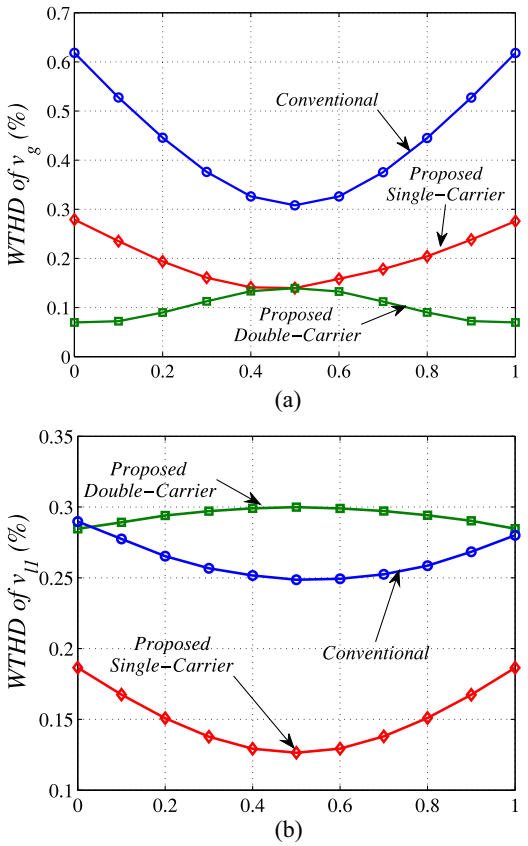

Fig. 10. (a) Weighted total harmonic distortion (WTHD) of rectifier voltage for the proposed and conventional configurations as a function of μ. (b) WTHD of the inverter voltage for the proposed and conventional configurations as a function of μ.

pulses are centered on the half period of the carrier signal. The change of the position of the voltage pulses leads also to change in the distribution of the zero instantaneous voltages similar to the distribution of the zero-voltage vector in the three-phase inverter [16], [19]. Consequently, μ_x, μ_y, and μ_z influence the harmonic distortion of the voltages generated by the converter, as well as its switching losses.

While Fig. 7 shows the modulation signals v_1^*, $v_{1a0_{12}}^*$, and v_x^* at the grid side considering μ_x, μ_y, and μ_z equal to 0, 0.5, and 1, Fig. 8 shows the voltages v_{ab}^*, $v_{2a0_{12}}^*$, $v_{4a0_{12}}^*$, and v_z^* at the machine side with the same sequence of μ_x, μ_y, and μ_z. Notice that at both cases, $\mu = 0.5$ guarantees sinusoidal carrier-based PWM with v_x^*, v_y^*, and v_z^* equal to zero, as shown in Figs. 7(b) and 8(b). On the other hand, when $\mu = 0$ or $\mu = 1$ leads a nonsinusoidal reference pole voltages, however, the resultant voltage v_1^* and v_{ab}^* are sinusoidal as shown in Figs. 7(a), 7(c), 8(a), and 8(c). Additionally, with $\mu = 0$ or $\mu = 1$, the distribution of zero instantaneous voltages are placed at the beginning or at the end of the switching period, respectively. The leading feature of PWM strategy with $\mu = 0$ or $\mu = 1$ is a reduction of the switching frequency. For the single-phase converter, there is no switching for a range of 180° while for the three-phase converter there is no switching for a range of 30°, reducing switching losses.

IV. Control Strategy

A. Control Block Diagram

The proposed converter has the same objectives as in the conventional converter, as observed in Fig. 1(b), i.e., 1) dc-link

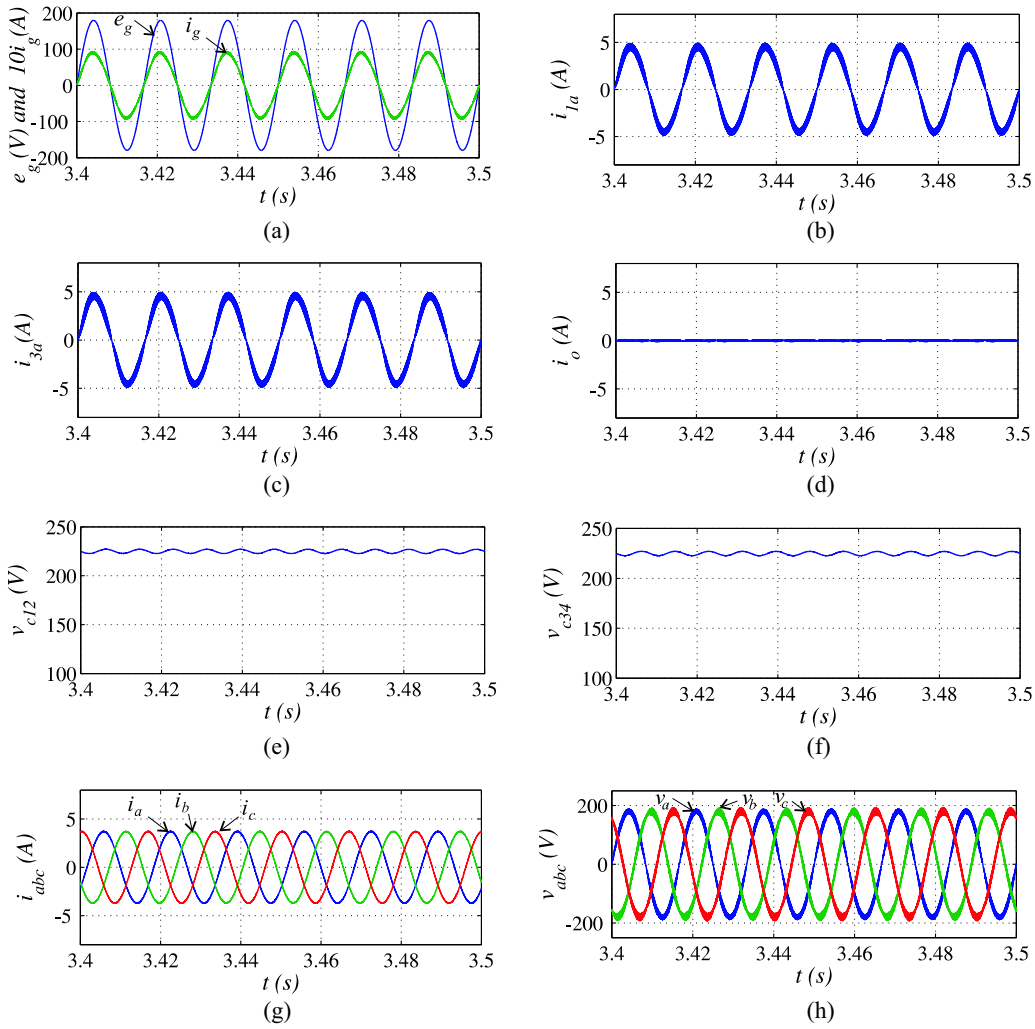

Fig. 11. Simulation results: (a) voltage and current of the grid, (b) input current of the converter 1, (c) input current of the converter 2, (d) circulating current, (e) dc-link voltage in C_{12}, (f) dc-link voltage in C_{34}, (g) load currents, and (h) load voltages.

voltage control, 2) power factor correction, and 3) three-phase voltage generation at the output-converter side. Additionally, the converter control of the proposed system needs to control the circulating current.

Fig. 9 presents the control block diagram for the proposed system. The capacitor dc-link voltages $v_{C_{12}}$ and $v_{C_{34}}$ are adjusted to their reference values $v^*_{C_{12}}$ and $v^*_{C_{34}}$ using controllers $R_{C_{12}}$ and $R_{C_{34}}$ (conventional PI-type controllers), respectively. Those controllers provide the amplitude of reference currents i^*_{1a} and i^*_{3a}. To control power factor and harmonic content at the input-converter side, the instantaneous reference currents i^*_{1a} and i^*_{3a} are synchronized with the grid voltage, as given in [23]. The blocks $G - i_{g1}$ and $G - i_{g3}$ have two functions, i.e., synchronization with the grid (through a phase-locked loop scheme) and generation of the sinusoidal reference currents. The control of the rectifier currents are implemented by using the controllers indicated by blocks R_1 and R_3. Those current controllers can be implemented by using linear or nonlinear techniques [24]–[26]. In this paper, we have used double sequence synchronous controllers [27], as discussed next.

The current controllers define the input reference voltages v^*_1 and v^*_3, which has been used in the PWM strategy. The homopolar current i_o is controlled by using the controller R_o, that determines voltage v^*_o. Inverter voltages are defined by the induction machine control, with the zero homopolar voltage.

B. Double Sequence Synchronous Controller

When the current is sinusoidal, a standard PI stationary controller does not guarantee zero sinusoidal steady-state error. A double sequence synchronous controller for ac variables were used to overcome such difficulty. The simplified controller has the following continuous-time control law:

$$\frac{dx_a}{dt} = x_b + 2k_i\xi_{sm} \tag{73}$$

$$\frac{dx_b}{dt} = -\omega_e^2 x_a \tag{74}$$

$$v^*_m = x_a + k_p\xi_m. \tag{75}$$

In these equations, $\xi_m = i^*_{ma} - i_{ma}$ is the current error ($m = 1$ or $m = 3$) for the rectifier current, respectively; x_a and x_b are

state-variables of the controller; v_m^* is the reference voltages; ω_e is the current reference frequency; and k_p and k_i are the gains of the controller. This controller gives zero error in the frequency ω_e.

The discrete-time version of controller is given by

$$x_a(k) = \cos(\omega_e h)\, x_a(k-1) + \frac{1}{\omega_e}\sin(\omega_e h)\, x_b(k-1) + 2k_i \frac{1}{\omega_e}\sin(\omega_e h)\, \xi_m(k-1) \tag{76}$$

$$x_b(k) = -\omega_e \sin(\omega_e h)\, x_a(k-1) + \cos(\omega_e h)\, x_b(k-1) + 2k_i\left[\cos(\omega_e h) - 1\right] \xi_m(k-1) \tag{77}$$

$$v_m^*(k) = x_a(k) + k_p \xi_m(k) \tag{78}$$

where h is the sampling period. Equations (73)–(78) were presented in [28].

When the load is balanced and a controller is employed to control the load current, the use of a single synchronous reference frame has been proven to be the best choice [28]. However, the use of a single reference frame is not the best choice when there is unbalancing in the system. The controller structure used in this paper is based on the utilization of two different synchronous controllers: the positive-sequence synchronous controller (rotating at ω_e) and the negative-sequence synchronous controller (rotating at $-\omega_e$). Both controllers operate simultaneously and their outputs are added.

V. Harmonic Distortion

The WTHD has been computed by using

$$\text{WTHD}(p) = \frac{100}{a_1}\sqrt{\sum_{i=2}^{p}\left(\frac{a_i}{i}\right)^2} \tag{79}$$

where a_1 is the amplitude of the fundamental voltage, a_i is the amplitude of ith, harmonic and p is the number of harmonics taken into consideration.

Fig. 10(a) shows the WTHD of the voltage generated by rectifier [$\frac{v_1+v_3}{2}$ for proposed configuration and $v_g = v_{g10} - v_{g20}$ for conventional configuration [see Fig. 3(b)] as a function of μ. The voltage generated by the rectifier is responsible to control i_g, which means that, this voltage is used to regulate the harmonic distortion of the utility grid.

Notice that, with both single- and double-carrier based PWM strategies, the WTHD of the input voltage is always lower than that in the conventional one, and for a particular case in which $\mu = 0.5$, the WTHD is the same for both methods (single and double carrier), but for the other values of μ the WTHD of the proposed converter with double-carrier strategy is lower than that with a single carrier.

On the other hand, the WTHD of the output voltage shows that [see Fig. 10(b)] the single-carrier-based PWM is the best option of implementation in the output-converter side.

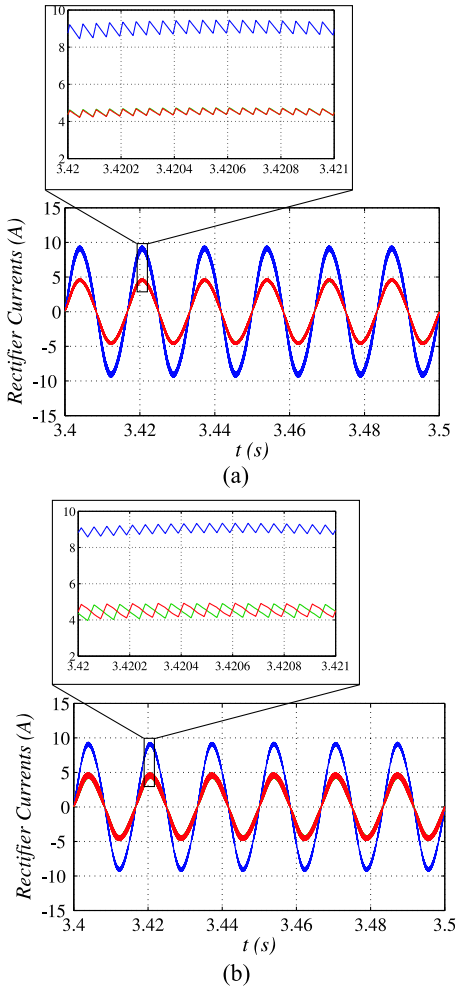

Fig. 12. Simulated results: (a) single-carrier-based PWM with $\mu = 0.5$ and (b) double-carrier-based PWM with $\mu = 0$.

VI. Simulation Results

The simulation results were obtained with the grid- and machine-phase voltages equal to 127 V_{rms}, dc-link voltage of 225 V, capacitance of 2200 μF, and input inductor filters with resistance and inductance given respectively by 0.1Ω and 2.6 mH. The load power was of 5 kVA.

Fig. 11 shows selected simulation results for the proposed system. Such results were collected using double-carrier-based PWM with $\mu = 0$ [the best case for WTHD—see Fig. 10(a)] for the input converters (converters 1 and 3), while a single-carrier-based PWM with $\mu = 0.5$ [the best case for WTHD—see Fig. 10(b)] is employed for the output converters (converters 2 and 4). Fig. 11 highlights the main control objectives handled by the proposed single-phase to three-phase power converter. Fig. 11(a) shows the ability of the proposed converter to control the grid current with a sinusoidal waveform and power factor close to one. While Fig. 11(b) and (c) demonstrate that the input-rectifier currents (i_{1a} and i_{3a}) are in fact half of the grid current due to the parallel connection at the grid side, Fig. 11(d) shows the control of the circulating current. Both dc-link voltages are under control, as observed in Fig. 11(e) and (f). As expected,

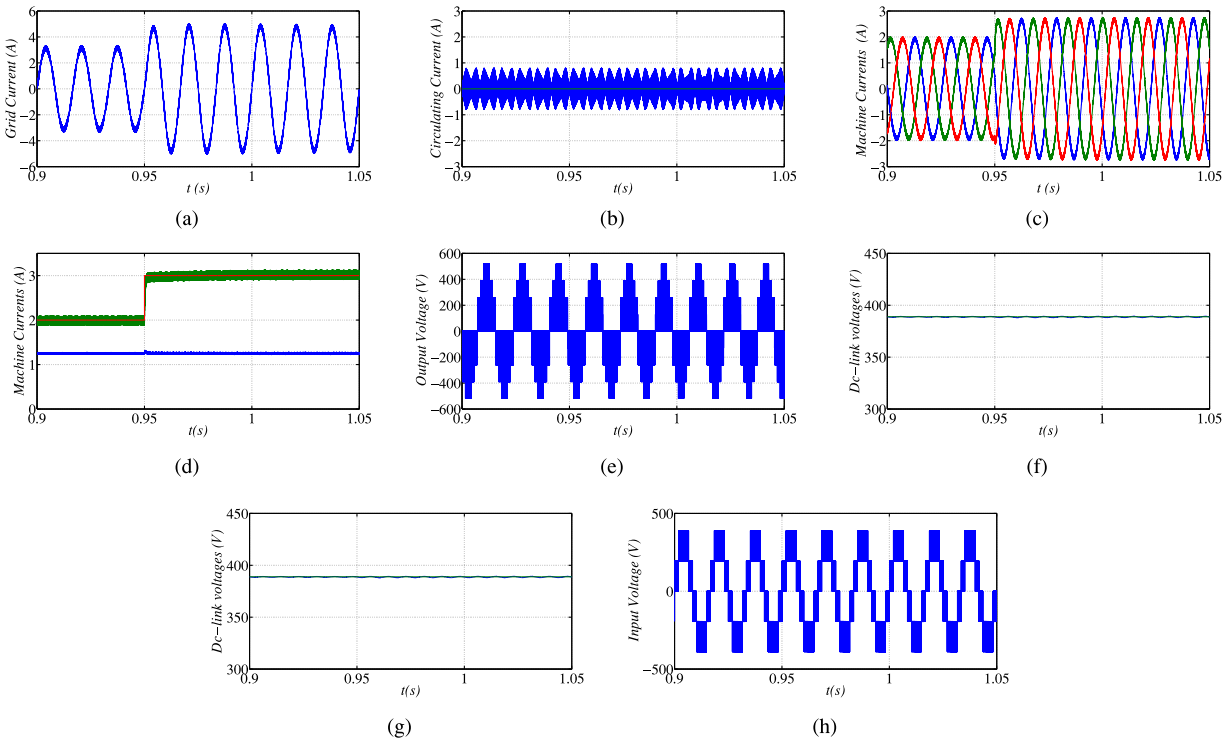

Fig. 13. Simulation results with current transient: (a) grid current (i_g), (b) circulating current (i_o), (c) machine currents, (d) current components i_{sd} and i_{sq}, (e) output voltages without LPF, (f) dc-link voltage (v_{C12}), (g) dc-link voltage (v_{C34}), and (h) input voltage.

there is a pulsating power at the dc-link capacitors due to the type of power from the single-phase grid. Since the three-phase power demanded by the three-phase machine is constant, the oscillating power from the grid appears at the capacitors. Fig. 11(g) and (h) show the currents and voltages of the machine. Notice that the load voltages were filtered with a low-pass filter (LPF) to prove the converter's capability to generate 127 V_{rms}.

Fig. 12 presents another set of simulated results to demonstrate the effect of the PWM strategies at the input side of the converter variables. In this case, the parameters of the three-phase machine were $r_s = 3\,\Omega$, $l_s = 14.0$ mH, $r_r = 3\,\Omega$, $l_r = 14.9$ mH, $l_m = 59.9$ mH, and two poles. The dc-link capacitors are given by 4400 μF. This is indeed the parameters of the three-phase machine employed on the experimental results. Fig. 12(a) and (b) shows the rectifier currents i_g, i_{1a}, and i_{3a} with a zoom to emphasize the use of either a single- or double-carrier PWM. Notice that the double-carrier-based PWM with $\mu = 0$ is equivalent to the interleaved approach, which allows ripple reduction.

Fig. 13 shows simulation results with a step transient on the i_{sq} component from $2A$ to $3A$, the component i_{sd} was kept constant. Since there is a step transient at the load side with the increase of the current, more energy will be delivered by the energy source, as observed in Fig. 13(a). The variables under control, such as circulating current [see Fig. 13(b)] and dc-link voltages [see Fig. 13(c) and 13(d)], keep following their references even with the hard transient presented in Fig. 13(c) and (d). It is worth mentioning that oscillation of the dc-link capacitor voltages are reduced as compared to Fig. 11(f) and (g) due to the higher value of capacitance. Fig. 13(e) and (h), in turn, show the output and input voltages generated by the converters without the LPF.

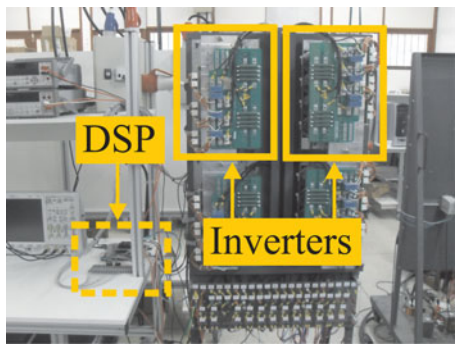

Fig. 14. Photo of the experimental setup.

VII. Experimental Results

The system in Fig. 5 has been implemented in the laboratory. The setup for the experimental tests is based on IGBTs from SEMIKRON controlled by a digital signal processor TMS320F28335 with a microcomputer equipped with appropriate plug-in boards and sensors. Fig. 14 shows a photo of the experimental setup. The machine used in the experimental setup has same parameter of the machine used in simulation results. The dc-link capacitors (C), switching frequency (f), and input inductors (L_g) are given by $C = 4400\ \mu$F, $f = 10$ kHz, and $L_g = 6$ mH, respectively, the grid, machine, and dc-link voltages are equal to 35 Vrms, 110 Vrms, and 195 V, respectively and the frequency machine was 30 Hz.

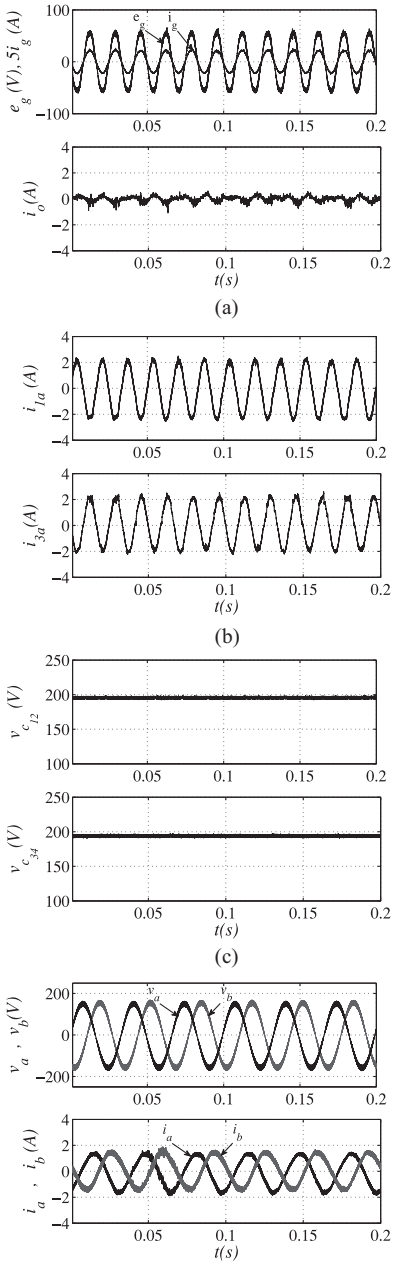

Fig. 15. Experimental results of the proposed configuration. (a) Voltage and current of the grid (top), and circulating current (bottom). (b) Input currents in converters 1 and 3 (i_{1a} and i_{3a}). (c) DC-link voltage of each capacitor. (d) Load voltages and currents of the motor.

The system shown in Fig. 5 has been implemented in the laboratory. Steady-state experimental results for the proposed configuration are shown in Fig. 15. The waveforms in this figure are: 1) (top) grid voltage (e_g) and grid current (i_g) and (bottom) circulating current (i_o), 2) input currents of the converters 1 and 3 (i_{1a} and i_{3a}), 3) dc-link voltage of each capacitor bank, and 4) (top) voltages and (bottom) currents of the three-phase motor with open-end motor winding connection.

Fig. 16 shows experimental results for the proposed configuration highlighting the interleaved operation. Fig. 16(a), (b), and (c) depict respectively, grid and rectifiers currents, zoom of the point 1, and zoom of the point 2.

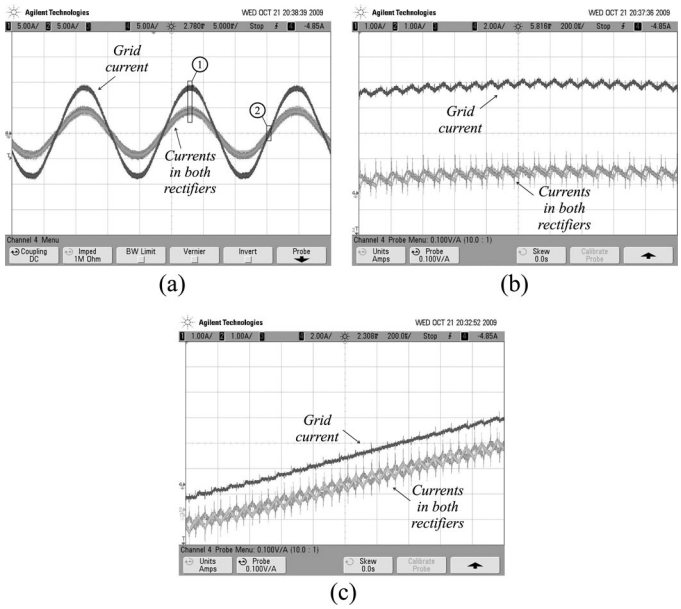

Fig. 16. Experimental results of the rectifier waveforms.

VIII. Conclusion

In this paper was proposed a single-phase to three-phase power conversion system with parallel rectifier and series inverter to cope with single-phase to three-phase asymmetry. Such converter guarantees both reduction in the input current processed by the rectifier circuit (due to the parallel connection) and reduction of the output voltage processed by each inverter (due to the series connection). In spite of proposing a topology with features not yet observed in the technical literature, this paper presented a comprehensive model of the proposed converter, modulation strategy, and a general comparison with the conventional configuration. Experimental results are used for the validation purpose.

References

[1] A. H. Maggs, "Single-phase to three-phase conversion by the ferraris-arno system," *Electr. Eng.—Part I, General, J. Inst.*, vol. 93, no. 32, pp. 133–136, Aug. 1946.

[2] K. Hisano, H. Kobayashi, and T. Kobayashi, "A new type single-phase to three-phase converter," *IEEE Trans. Magn.*, vol. 2, no. 3, pp. 643–647, Sep. 1966.

[3] S. Dewan and M. Showleh, "A novel static single-to three-phase converter," *IEEE Trans. Magn.*, vol. 17, no. 6, pp. 3287–3289, Nov. 1981.

[4] M. Liserre, "Dr. Bimal K. Bose: A reference for generations [editor's column]," *IEEE Ind. Electron. Mag.*, vol. 3, no. 2, pp. 2–5, Jun. 2009.

[5] F. Blaabjerg, A. Consoli, J. A. Ferreira, and J. D. van Wyk, "The future of electronic power processing and conversion," *IEEE Trans. Ind. Appl.*, vol. 41, no. 1, pp. 3–8, Jan./Feb. 2005.

[6] F. W. Gutzwiller, "Thyristors and rectifier diodes-the semiconductor workhorses," *IEEE Spectrum*, vol. 4, no. 8, pp. 102–111, Aug. 1967.

[7] A. Elasser, M. H. Kheraluwala, M. Ghezzo, R. L. Steigerwald, N. A. Evers, J. Kretchmer, and T. P. Chow, "A comparative evaluation of new silicon carbide diodes and state-of-the-art silicon diodes for power electronic applications," *IEEE Trans. Indust. Appl.*, vol. 39, no. 4, pp. 915–921, Jul./Aug. 2003.

[8] M.-K. Nguyen, Y.-G. Jung, and Y.-C. Lim, "Single-phase AC–AC converter based on quasi-z-source topology," *IEEE Trans. Power Electron.*, vol. 25, no. 8, pp. 2200–2210, Aug. 2010.

[9] M.-K. Nguyen, Y. cheol Lim, and Y.-J. Kim, "A modified single-phase quasi-z-source AC–AC converter," *IEEE Trans. Power Electron.*, vol. 27, no. 1, pp. 201–210, Jan. 2012.
[10] B. Saint, "Rural distribution system planning using smart grid technologies," in *Proc. Rural Electric Power Conf.*, Apr. 2009, pp. B3-1–B3-8.
[11] A. R. C. de Lima Montenegro Duarte, U. H. Bezerra, M. E. de Lima Tostes, and G. N. da Rocha Filho, "Alternative energy sources in the Amazon," *IEEE Power Energy Mag.*, vol. 5, no. 1, pp. 51–57, Jan./Feb. 2007.
[12] X. Wang, H. Zhong, Y. Yang, and X. Mu, "Study of a novel energy efficient single-phase induction motor with three series-connected windings and two capacitors," *IEEE Trans. Energy Convers.*, vol. 25, no. 2, pp. 433–440, Jun. 2010.
[13] M. Khan, I. Husain, and Y. Sozer, "Integrated electric motor drive and power electronics for bidirectional power flow between the electric vehicle and DC or AC grid," *IEEE Trans. Power Electron.*, vol. 28, no. 12, pp. 5774–5783, Dec. 2013.
[14] Y.-S. Lai, W.-T. Lee, Y.-K. Lin, and J.-F. Tsai, "Integrated inverter/converter circuit and control technique of motor drives with dual-mode control for EV/HEV applications," *IEEE Trans. Power Electron.*, vol. 29, no. 3, pp. 1358–1365, Mar. 2014.
[15] C. B. Jacobina, E. C. dos Santos, Jr, N. Rocha, and E. L. Lopes Fabricio, "Single-phase to three-phase drive system using two parallel single-phase rectifiers," *IEEE Trans. Power Electron.*, vol. 25, no. 5, pp. 1285–1295, May 2010.
[16] C. Jacobina, E. Cipriano dos Santos, N. Rocha, de Sa, B. Gouveia, and E. da Silva, "Reversible ac drive systems based on parallel ac-ac dc-link converters," *IEEE Trans. Ind. Appl.*, vol. 46, no. 4, pp. 1456–1467, Jul./Aug. 2010.
[17] Y. Ohnuma and J. I. Itoh, "A control method for a single-to-three-phase power converter with an active buffer and a charge circuit," in *Proc. Energy Convers. Congr. Expo.*, Sep. 2010, pp. 1801–1807.
[18] Y. Ohnuma and J. Itoh, "Space vector modulation for a single phase to three phase converter using an active buffer," in *Proc. Int. Power Electron. Conf.*, Jun. 2010, pp. 574–580.
[19] J. Holtz, "Pulsewidth modulation for electronic power conversion," *Proc. IEEE*, vol. 82, no. 8, pp. 1194–1214, Aug. 1994.
[20] A. M. Trzynadlowski, R. L. Kirlin, and S. F. Legowski, "Space vector PWM technique with minimum switching losses and a variable pulse rate," *IEEE Trans. Ind. Electron.*, vol. 44, no. 2, pp. 173–181, Apr. 1997.
[21] O. Ojo and P. M. Kshirsagar, "Concise modulation strategies for four-leg voltage source inverters," *IEEE Trans. Power Electron.*, vol. 19, no. 1, pp. 46–53, Jan. 2004.
[22] C. B. Jacobina, A. M. N. Lima, E. R. C. da Silva, R. N. C. Alves, and P. F. Seixas, "Digital scalar pulse-width modulation: A simple approach to introduce non-sinusoidal modulating waveforms," *IEEE Trans. Power Electron.*, vol. 16, no. 3, pp. 351–359, May 2001.
[23] M. Malinowski, M. P. Kazmierkowski, and A. M. Trzynadlowski, "A comparative study of control techniques for PWM rectifiers in AC adjustable speed drives," *IEEE Trans. Power Electron.*, vol. 18, no. 6, pp. 1390–1396, Nov. 2003.
[24] P. Verdelho and G. D. Marques, "Four-wire current-regulated PWM voltage converter," *IEEE Trans. Ind. Electron.*, vol. 45, no. 5, pp. 761–770, Oct. 1998.
[25] H. Abu-Rub, J. Guzinski, Z. Krzeminski, and H. Toliyat, "Predictive current control of voltage-source inverters," *IEEE Trans. Ind. Electron.*, vol. 51, no. 3, pp. 585–593, Jun. 2004.
[26] G. Dong and O. Ojo, "Current regulation in four-leg voltage-source converters," *IEEE Trans. Ind. Electron.*, vol. 54, no. 4, pp. 2095–2105, Aug. 2007.
[27] C. B. Jacobina, M. B. de R. Correa, R. F. Pinheiro, E. R. C. da Silva, and A. M. N. Lima, "Modeling and control of unbalanced three-phase systems containing PWM converters," *IEEE Trans. Ind. Appl.*, vol. 37, no. 6, pp. 1807–1816, Nov./Dec. 2001.
[28] C. B. Jacobina, M. B. R. Correa, T. M. Oliveira, A. M. N. Lima, and E. R. C. da Silva, "Current control of unbalanced electrical systems," in *Proc. IEEE Conf. Rec. Ind. Appl. Conf. Annu. Meet.*, 1999, pp. 1011–1017.

Euzeli Cipriano dos Santos Jr. (S'04–M'08–SM'12) received the B.S., M.S., and Ph.D. degrees in electrical engineering from the Federal University of Campina Grande, Campina Grande, Brazil, in 2004, 2005, and 2007, respectively.

From 2006 to 2007, he was with Electric Machines and Power Electronics Laboratory, Texas A&M University, College Station, TX, USA, as a Visiting Scholar. From August 2006 to March 2009, he was the Professor at the Federal Center of Technological Education of Paraíba, Brazil. From December 2010 to March 2011, he was a Visiting Professor at the University of Siegen, Germany, sponsored by DAAD/CAPES. From March 2009 to July 2012, he was with the Department of Electrical Engineering, Federal University of Campina Grande. Since July 2012, he has been with the Indiana University—Purdue University Indianapolis, where he is currently an Assistant Professor of electrical engineering. His research interests include power electronics, renewable energy systems, and electrical drives.

Nady Rocha (M'10) was born in 1982, Bahia, Brazil. He received the B.S., M.S., and Ph.D. degrees in electrical engineering from the Federal University of Campina Grande, Campina Grande, Brazil, in 2006, 2008, and 2010, respectively.

Since 2011, he has been with the Department of Electrical Engineering, Federal University of Paraíba, João Pessoa, Brazil, where he is currently an Associate Professor of electrical engineering. His research interests include power electronics and electrical drives.

Cursino Brandão Jacobina (S'78–M'78–SM'98–F'14) was born in Correntes, Brazil, in 1955. He received the B.S. degree in electrical engineering from the Federal University of Paraíba, Campina Grande, Brazil, in 1978, and the Diplôme d'Etudes Approfondies and the Ph.D. degrees from the Institut National Polytechnique de Toulouse, Toulouse, France, in 1980 and 1983, respectively.

From 1978 to March 2002, he was with the Department of Electrical Engineering, Federal University of Paraíba. Since April 2002, he has been with the Department of Electrical Engineering, Federal University of Campina Grande, Campina Grande, where he is now a Professor of electrical engineering. His research interests include electrical drives, power electronics, and energy systems.